

# BEAM INSTRUMENTATION CHALLENGES FOR FCC-ee

E. Carideo, T. Lefevre, S. Mazzoni, A. Schlägelhofer, M. Wendt\*, CERN, Geneva, Switzerland  
 B. Häger, G. Niehues, M. Reißig, A.-S. Müller, KIT, Karlsruhe, Germany  
 U. Iriso, ALBA-CELLS, Bellaterra, Spain  
 T. Mitsuhashi, KEK, Tsukuba, Japan  
 M. Siano, University of Milano, Milano, Italy

## Abstract

For the accelerator-based future of high energy physics at the energy frontier, CERN started to investigate a 92 km circumference Future Circular Collider (FCC), as e<sup>+</sup>/e<sup>-</sup> collider the FCC-ee will operate at beam energies up to 182.5 GeV. Beside the machine operational aspects, beam instrumentation will play a key role in verifying and optimizing the machine to achieve the ambitious beam parameters and quality. This paper gives a brief overview of the various challenges to develop the required beam instruments, with focus on beam position, beam size and bunch length measurements, and well as an outline of the planned R&D activities.

## INTRODUCTION

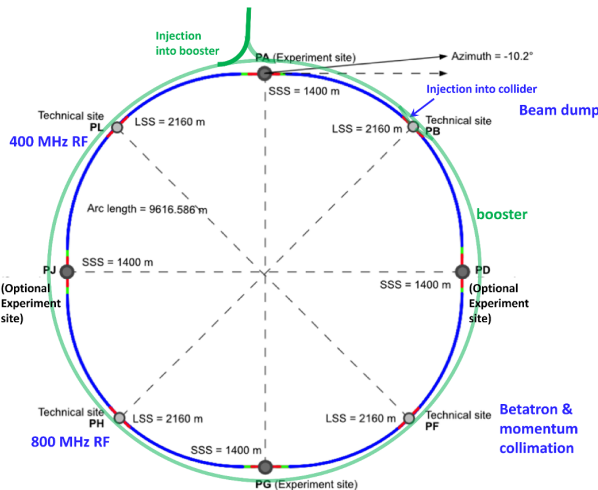


Figure 1: Layout of the main rings of FCC-ee.

The FCC-ee project [1] consists of two main rings and a booster ring in a tunnel of approximately 92 km circumference, plus the injectors and a positron source. For this discussion on the challenges and requirements of the FCC-ee beam instrumentation we focus on the main rings, see Fig. 1, which – with exception of the large circumference – has many aspects in common with 4<sup>th</sup>-generation synchrotron light sources.

Table 1 lists those FCC-ee beam parameters which are particular relevant for the beam instrumentation, with the red highlighted values presenting the biggest challenges.

Table 1: FCC-ee beam parameters relevant to beam instrumentation.

Parameter (4 IPs, $t_{rev} = 304 \mu\text{s}$ )	Value
circumference [km]	91.18
max. beam energy [GeV]	182.5
max. beam current [mA]	1280
max. # of bunches/beam	10000
min. bunch spacing [ns]	25 (15)
max. bunch intensity [ $10^{11}$ ]	2.43
min. H geometric emittance [nm]	0.71
min. V geometric emittance [pm]	1.42
min. H rms IP spot size [ $\mu\text{m}$ ]	8
min. V rms IP spot size [nm]	34
min. rms bunch length SR/BS [mm]	1.95 / 2.75

## BEAM POSITION MEASUREMENT

The two main rings and the booster ring together will need a total of approximately 7000 beam position monitors (BPM), distributed along the ~90 km FCC-ee tunnel. In the arcs, the preferred location of the button-style BPM pick-ups is next to the quadrupole, with the BPM body rigidly fixed to the pole shoes at one end of the magnet. An study currently investigates the integration of the BPM pickup with the quadrupole in a way that no extra space is required. While many details of the four, symmetrically arranged BPM pickup electrodes still need to be developed, a study to optimize new manufacturing processes of the the BPM body with the vacuum chamber made out of copper, together with the button RF UHV feedthrough have been initiated, see also Fig. 2.

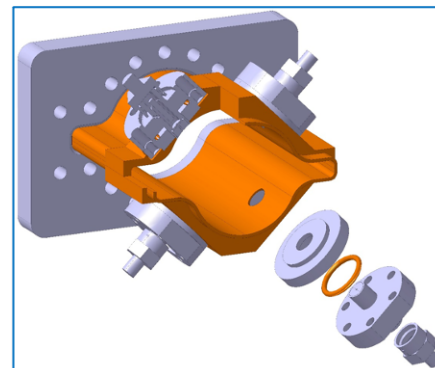


Figure 2: Manufacturing R&D for FCC-ee BPM pickups.

\* manfred.wendt@cern.ch

Being one of the large scale beam instrumentation systems, the FCC-ee BPM system not only needs to fulfill the core requirements like resolution and accuracy, but also has to be optimized along other aspects, such as segmentation of read-out electronics in the tunnel, costs, maintenance aspects, integration with other systems like RF, timing signals, corrector magnet power supplies, etc. The beam position data from BPM system will be used for the beam orbit feedback, therefore latency effects need to be considered.

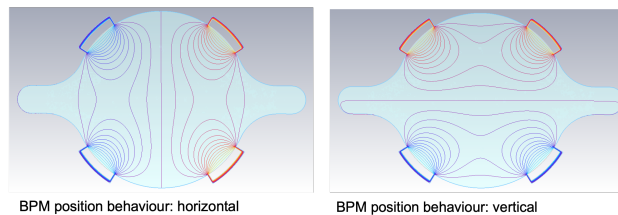


Figure 3: Lines of constant beam displacement of a button BPM, horizontal (left), vertical (right).

### BPM Requirements

Some of the basic requirements for the BPM system have been discussed during the workshop and since, and of course, a formal BPM requirement document still has to be drafted. While some of those requirements are similar to those of the 4<sup>th</sup>-generation synchrotron light sources, the 70 mm diameter of the FCC-ee vacuum chamber with its “winglets” for the synchrotron light absorption is substantially larger, therefore results in a reduced the position sensitivity of the BPM, which is slightly below  $2/R$  (with  $R = 35$  mm) near the center of the vacuum chamber due to the “rotated” BPM pickup electrodes, see also Fig. 3.

Similar to the present LHC BPM system, the FCC-ee BPMs need to acquire bunch-by-bunch and turn-by-turn beam positions in a synchronized fashion, and report the beam orbit average value of the position data for all bunches in a turn over many turns. We currently assume a minimum bunch spacing of 25 ns for the FCC-ee, however, that value may be reduced down to 15 ns, see Table. 1.

**Resolution** A BPM orbit resolution of  $<1\text{ }\mu\text{m}$  is anticipated, while the turn-by-turn resolution should achieve  $10\text{ }\mu\text{m}$ .

**Accuracy** A relative accuracy, i.e. not accounting for the BPM offset, in the range  $1 \dots 10\text{ }\mu\text{m}$  seems feasible, but requires a correction of the non-linearities of the BPM pickup, see also Fig. 3.

**Alignment & roll errors** A stretched-wire based, electromagnetic pre-alignment of the integrated BPM-quadrupole module can substantially reduce alignment errors and allows to evaluate offset and roll-errors between the electromagnetic center of the BPM pickup and the magnetic center of the quadrupole [2–5]. Simulations indicate that alignment errors with  $x$ ,  $y$ -offsets of  $\sim 10\text{ }\mu\text{m}$  and rolls of  $10 \dots 30\text{ }\mu\text{rad}$  can be tolerated.

### IP BPM's

With nanometer beam size beams at the interaction point (IP), design and integration of the BPM's in the superconducting (SC) final focus quadrupoles becomes mission critical. Fortunately the e<sup>+</sup>/e<sup>-</sup> beam are already separated entering the final focus segmented SC quadrupole, therefore also those 3+3 BPMs pickups (per beam) can be realized as button-style. The warm bore of the quadrupole simplifies to some extend the challenges of the pickup, however, alignment, integration including cable routing and long-term stability issues need to be studied in detail as those BPMs have the tightest requirements.

### Wakefield and Beam-Coupling Impedance

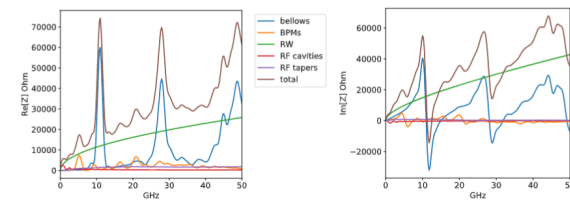


Figure 4: Real (left) and imaginary (right) part of beam-coupling impedance of different devices. The total impedance is the sum of all the contributions.

Improving the accuracy of the beam impedance model of an accelerator is important to minimize beam instabilities and keep power losses under control. The total beam-coupling impedance for the FCC-ee, as well as the contribution of each device, is shown in Fig. 4 and in [6] the method utilised to calculate them is described.

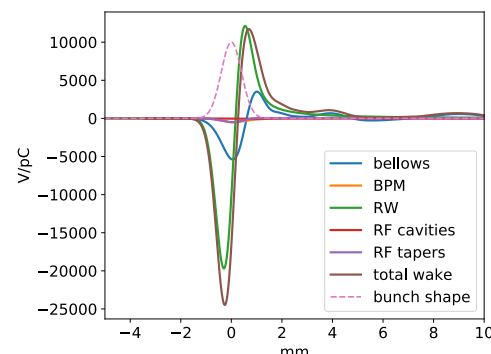


Figure 5: Wake potential of a 0.4 mm Gaussian bunch due to different devices and used as input for beam dynamics simulations.

We have calculated the contribution of impedance model of the machine devices that have been evaluated until now, shown in Fig 5. A major contributor to the total beam-coupling impedance is the resistive wall (RW) impedance of the beam pipe and bellows with the RF fingers necessary to guarantee good electrical contact between sections of the beam pipe. For the other devices, just the beam position

monitors show a small peak around 5 GHz, Fig.4 but we have to remind that this study is still a work in progress. For the moment, for the total contribution to the impedance budget the real number of bellows is still unknown but to be conservative we decided to overestimate the number of bellows distributed along the machine to 20000. In addition to the resistive wall and bellows, we also evaluated the contribution due to the 400 MHz RF system, consisting out of 52 single cell cavities arranged in groups of 4 for each cryomodule, which has, at each end, a 500 mm long taper section to ensure a smooth transition between the 50 mm and the 150 mm circular pipes inside the cryomodule. Finally, also the 4000 BPMs of the two main rings have been taken into account [7].

## BEAM LOSS MEASUREMENT

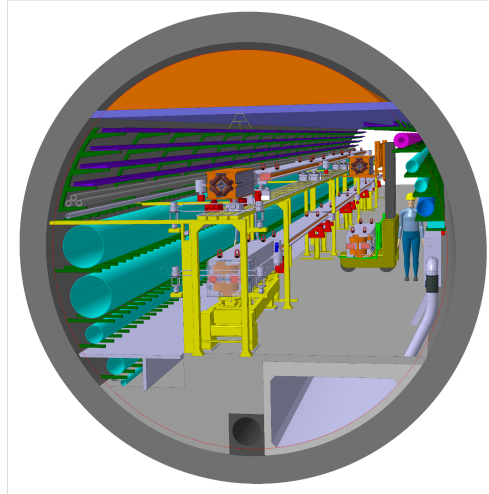


Figure 6: FCC-ee tunnel layout.

Dedicated R&D activities on the beam loss monitors (BLM) for the FCC-ee have not yet been started. However, the large energy stored in both, the two main rings and the booster ring requires a well defined machine protection system (MPS), which needs to be supported by a BLM system. For the BLMs, several challenges need to be addressed:

- Distributed large scale system, consisting out of several thousand beam loss monitors.
- The BLMs in the FCC-ee arcs need to be insensitive to X-rays.
- The beam losses from the individual rings in the FCC-ee tunnel need to be identified. Figure 6 shows the close proximity of the three accelerator rings.

Several ideas are discussed to address the last point, to distinguish the beam losses – which expect to appear mostly near the quadrupole magnets – between the individual rings. An arc layout with the location of the booster quadrupoles longitudinally staged between the main ring quadrupoles would certainly help to address the problem.

Some of the BLM R&D done for Compact Linear Collider (CLIC) addresses the issue to disentangle losses from counter-travelling beams in close proximity [8–10], and recent studies of “optical Cherenkov fibers” at the CERN CLEAR beam test facility show promising results to detect particle losses with high directivity, see the principle illustrated in Fig. 7.

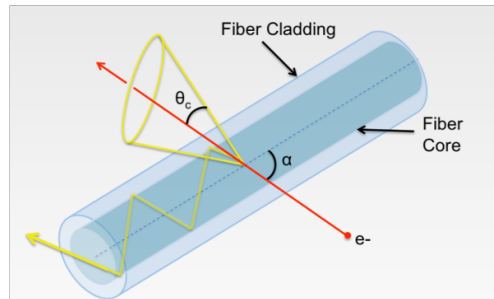


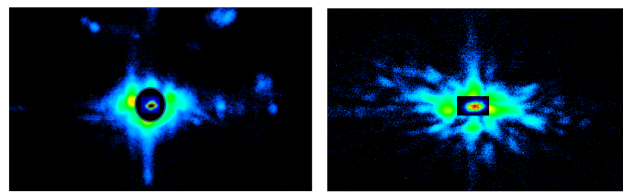
Figure 7: Cherenkov radiation from an optical fiber used as beam loss detector.

## BEAM SIZE MEASUREMENT

A variety of R&D activities address the measurement of the small transverse beam size, which in the case of FCC-ee are as small as 5 . . . 7 μm in the vertical plane. The main challenges are then linked to the use of very high energy beams for which synchrotron radiation will suffer from diffraction effects and would require the use and detection of high energy X-rays. In addition, the small bending angle of main dipoles would make the photon extraction line particularly long and the very large beam current would also put high constraints on the impedance and heat load of the photon extraction vacuum vessel (mirrors and windows).

### Beam Size Measurement R&D at KEK

**Development of poly-crystal Diamond mirror for the SR monitor of FCC ee by using the SuperKEKB SR monitor** The remarkable idea of a “single crystal diamond mirror” was developed as synchrotron radiation (SR) extraction mirror for SuperKEKB [11]. Diamond has an outstanding thermal conductivity, enabling to solve the biggest problem “how to suppress thermal deformation”. But we still face the problem, thickness and size are limited to 0.5 mm and 10 mm × 10 mm, and due to this limit, we could not make a large mirror in the required high optical quality. Recently, an optical quality poly-crystal diamond material was developed and realized as larger and thicker bulk mirror. Using this material, a mirror of size 20 mm × 30 mm and 2 mm thickness was manufactured and tested in the SuperKEKB high energy ring (HER) SR monitor. The result of the optical testing showed a surface flatness is better than  $\lambda/5$ . The deformation during irradiation of SR was measured using a hole-array mask. As result, no significant deformation was observed for a beam current of 1200 mA in the storage ring. This mirror is now regularly used as SR monitor for SuperKEKB.



(a) HER,  $I_{beam} = 0.57$  mA      (b) LER,  $I_{beam} = 0.61$  mA

Figure 8: Beam halo measurement at SuperKEKB, using a diamond mirror for the SR extraction.

**Development of the coronagraph with long-focus *Gregorian* telephoto-objective system for beam halo observation** For the observation of the beam halo a coronagraph was developed and manufactured. The coronagraph has three stages of optical systems, the objective system, the re-diffraction system and the relay system. Since the SR monitor should have a long optical path (a few hundred meter), we need an objective system with a long focal length [12]. Moreover, the entrance aperture is determined by the extraction mirror. Therefore, we must assign this aperture for the entrance pupil of the objective system. To satisfy these two conditions we developed a coronagraph with a reflective telephoto system based on the *Gregorian* telescope for the objective system to be utilized at SuperKEKB. The focal length is designed to be 7028 mm and front principal point position is designed to be at the location of the extraction mirror. As a result of this construction, the performance of the objective system has a diffraction limited quality. The re-diffraction system and relay system are designed based on the *Kepler* type telescope. As result of the optical testing using the beams in the HER and LER, we achieved a contrast better than 6-orders of magnitude between the beam core and the background. The observation of beam halo in the HER proved to be rather simple, showing a smooth transition between the beam core continues to the beam tail, then to the halo, see Fig. 8a. In the LER we observed a more complicated distribution of beam halo as shown in Fig. 8b. In both Figures, 8a and 8b, the beam core image and the shadow of the opaque mask are superimposed to the halo image.

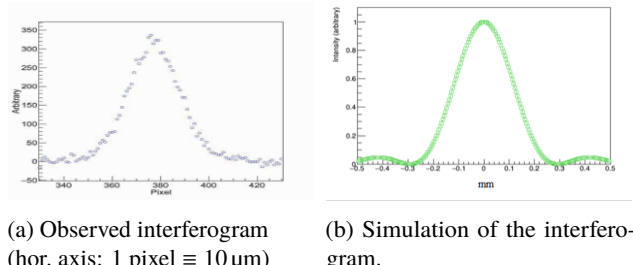


Figure 9: X-ray interferometer R&D at SuperKEKB, using an angular beam size of 2.7  $\mu$ rad.

**Development of a X-ray interferometer for the measurement of the apparent very small beam size in FCC-ee, using the X-ray monitor line in SuperKEKB** FCC-ee is very large machine with a large bending radius, which makes a long distance between the beam source point and the observation point at the SR monitor necessary 3). The expected apparent angular beam size (the apparent angular size of the beam is defined as  $\theta_s = \sigma/d$ , with  $\sigma$  being the beam size and  $d$  the distance between the beam source point and the observation point) in FCC-ee is around 0.05  $\mu$ rad. The best resolution achieved by popular instruments, such as the pinhole camera, the SR interferometer, etc. are about 0.5  $\mu$ rad, still not sufficient to measure the apparent very small beam size of the FCC-ee [13]. An X-ray interferometer promises for a very high resolution due to short wavelength of the X-rays, typically 0.1 nm. We developed an X-ray interferometer utilizing the X-ray monitor line in the HER of SuperKEKB. A double slit of 15  $\mu$ m in width and 30  $\mu$ m in separation, realized on a 20  $\mu$ m thick Au plate, was installed 10 m downstream the source point. The X-ray interferogram is observed 30 m downstream from the double slit by using a YAG fluorescence screen. The observation result of the interferogram for an angular beam size of 2.7  $\mu$ rad (measured by the X-ray coded aperture) is shown in Fig. 9a. For comparison, the result of a simulation of the interferogram is shown in Fig. fig:XraySim. Since interference fringe is smeared-out by the rather large beam size, we could not observe a sign of the interference fringe in this test. In the next beam studies we will try the investigate the X-ray interferometer for a beam size <1.5  $\mu$ rad.

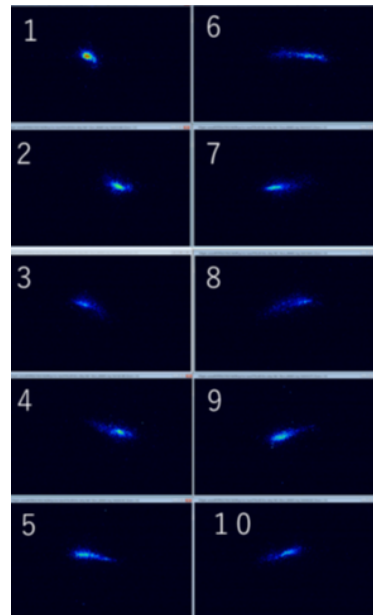


Figure 10: Profiles of the injected beam bunch for the 1<sup>st</sup> ten turns into the HER of SuperKEKB.

**Fast gated camera** Since the SuperKEKB operating tune is close to a half-integer, the bunches oscillate strongly

on a turn-by-turn basis. Utilizing the coronagraph, we can mask the stored beam profile. This setup enables to observe the injected beam profile in presence of stored beam. As a result of the observation of injected beam with a fast gated, image intensified camera, we now can measure the turn-by-turn instantaneous beam profile of a selected bunch. This apparatus is particularly valuable for observing the turn-by-turn injected beam profile [14, 15]. We used the *Gregorian* reflective objective system developed for the coronagraph to obtain the images of the injected beam profile at SuperKEKB [15]. Figure 10 shows the injected beam profile of turns #1 to #10 in the HER after injection. The bunch profile using the coronagraph is shown in Fig. 11. This observation is very helpful for the injection tuning.

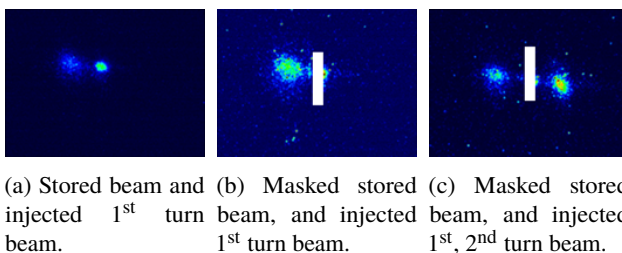


Figure 11: Injected beam profile measured with the coronagraph. In (b) and (c) the mask is indicated as white rectangle.

### Beam Size Measurement R&D – 2D Heterodyne Near-Field Speckles

Recently, we have developed a novel interferometric technique to perform full 2D coherence mapping of X-ray synchrotron radiation, thus full 2D beam size measurements [16]. The method relies on Fourier analysis of the Heterodyne Near Field Speckles (HNFS) formed by interfering the weak spherical waves scattered by nanoparticles suspended in water with the intense trans-illuminating X-ray beam. This peculiar interference generates a stochastic intensity distribution known as a speckle pattern. The spatial power spectrum of such speckles exhibits peculiar oscillations, known as Talbot oscillations [17], whose envelope allows direct mapping of the full 2D coherence function of the incoming synchrotron light [16, 18, 19]. The 2D beam profile, as well as the horizontal and vertical beam sizes, is then retrieved by the Fourier transform of the measured 2D spatial coherence, under the conditions of applicability of the Van Cittert and Zernike theorem [20]. More in general, approaches based on statistical optics should be adopted [16, 21].

We have validated the technique at the NCD-SWEET undulator beamline at the ALBA synchrotron light source through a systematic measurement of the horizontal and vertical beam sizes as a function of the machine coupling parameter [16]. The experimental setup is sketched in Fig. 12(a). It is marked by simplicity, and does not require any dedicated X-ray optics. A typical example of acquired X-ray speckles

is shown in Fig. 12(b), and the corresponding 2D power spectrum is reported in Fig. 12(c).

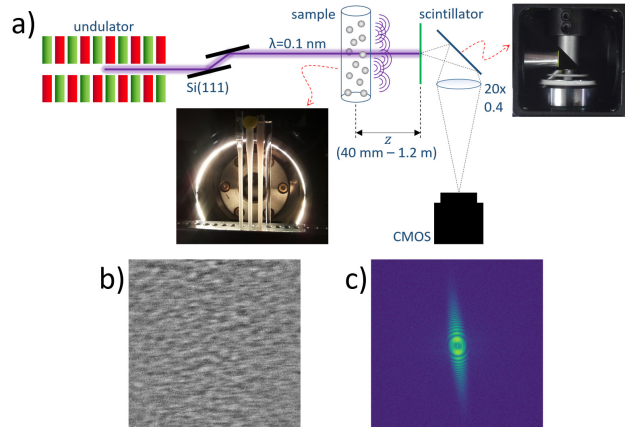


Figure 12: Sketch of the HNFS setup at the NCD-SWEET beamline at ALBA (a). Measured X-ray speckles (b) and corresponding power spectrum (c) with 12.4 keV photons.

Thanks to the 2D mapping of the HNFS method, we can unambiguously identify and assess the horizontal and vertical beam sizes even in presence of misaligned optics, as indicated in Fig. 12(c) by the tilt of the power spectrum. Results are reported in Fig. 13 alongside with theoretical predictions, and prove that the HNFS method can be employed as a reliable technique to measure transverse beam sizes in a wide range of sizes, from a few micrometers up to more than 100  $\mu\text{m}$ .

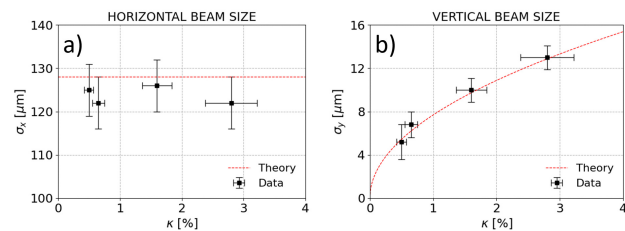


Figure 13: Measured horizontal (a) and vertical (b) beam size at the NCD-SWEET beamline as a function of the ALBA coupling parameter.

### Laser Wire Scanner

Laser Wire Scanners (LWS) have already demonstrated their ability to measure micron beam sizes [22]. They use high power lasers that would interact with the primary beams and produce Compton scattered photons and electrons/positrons. LWS will be based on the same technologies, laser and detectors as the ones developed for the FCCee Compton polarimeter [23]. A different laser-beam interaction vacuum chamber would actually required for LWS and will be studied in the future.

### BUNCH LENGTH MEASUREMENT

In the FCC-ee main rings, up to 10000, few mm long, bunches are colliding permanently. The amount of beam-

strahlung photons emitted during collision is large and generates an even larger increase in bunch length, up to 14 mm in the worse case scenario when colliding at 45 GeV beam energy. To maintain the collision rate at the highest level, a top-up injection scheme is proposed, injecting new short bunches in RF buckets populated with longer colliding bunches. To optimise this process, a precise knowledge of the longitudinal bunch profile along the ring is needed continuously. Different methods can be envisaged for that such as a photon counting techniques [24] or streak camera measurements [25] based on the measurement of visible photons emitted via Synchrotron radiation (SR) or *Cherenkov* diffraction radiation (ChDR). Techniques using electro-optical sampling and bi-refringent crystal are also discussed as well as frequency spectrum analysis using the emission of coherent radiation from short bunches at mm wavelength again using SR or ChDR [26]. In the paragraphs below, we present the status of the work being performed at the moment on Cherenkov Diffraction radiation and E-O detection in the context of FCC-ee, as well as streak camera measurements performed at KEK.

#### *Streak camera measurements at KEK*

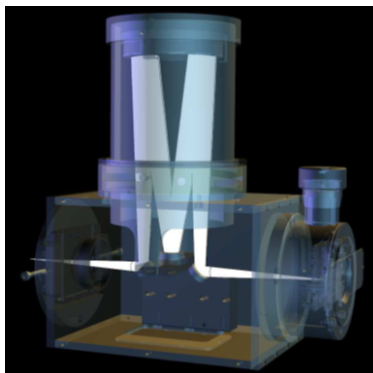


Figure 14: *Offner* relay reflective system for the streak camera reflective input optics.

The streak camera is an important tool to diagnose the temporal profile of the beam bunches in the optical diagnostic beam-line of SuperKEKB for bunches of typically 5...10 mm RMS length. The reduction of the chromatic aberration of the streak camera optics is one of the most important points in this measurement technique. For this purpose, typically a band-pass filter is used in the optical path, however, this reduces the light input intensity for low bunch intensities, which results in noisy, unreliable measurements. A different solution has been implemented using reflective optics. Therefore we have developed an *Offner* relay reflective system [27, 28]. Figure 14 shows a cutaway side view of the reflective input optics. Using this input optics, we can measure the bunch length down to low bunch intensities < 0.1 mA. A result of bunch length measurement at LER of SuperKEKB is shown in Fig. 15.

Another important application of the streak camera is the correlated spatial-temporal measurement of an electron

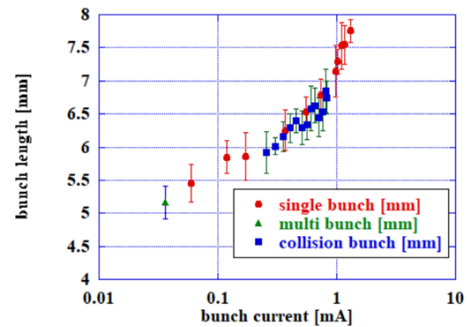


Figure 15: Bunch length measurement results at the LER of SuperKEKB.

bunch. This technique enables the observation of instabilities of the beam, such as head-tail oscillations, quadrupole oscillations, or the beam size blow-up due to the electron cloud instability, etc. [29]. Figure 16 shows the observation for quadrupole and head-tail oscillations at the KEK Photon Factory.

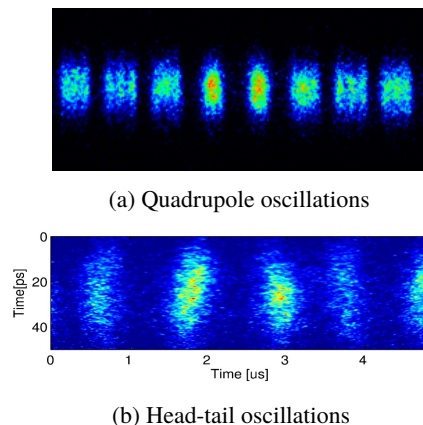


Figure 16: Correlated spatial-temporal streak camera measurements at the KEK Photon Factory.

#### *R&D based on Cherenkov Diffraction Radiation*

A charged particle moving in close vicinity to a dielectric generates Cherenkov diffraction radiation (ChDR) if its velocity  $v$  is greater than the speed of light in the dielectric material. Figure 17 illustrates this principle. The generated radiation is emitted at a well-defined angle  $\theta_{Ch} = \arccos[1/(n_1 \beta)]$  which is known as *Cherenkov* angle [30] and where  $n_1 = \sqrt{\epsilon_r \mu_r}$  denotes the refractive index of the dielectric and  $\beta = v/c$ .

The properties of ChDR are of high interest for beam diagnostic devices due to its high directivity, non-invasive characteristic and small form factor of radiators. Especially making use of the incoherent ChDR is a promising candidate for bunch-length diagnostics at FCC-ee. However, two analytical models [31, 32] predict different photon yields the higher the frequency, being far inside the incoherent part

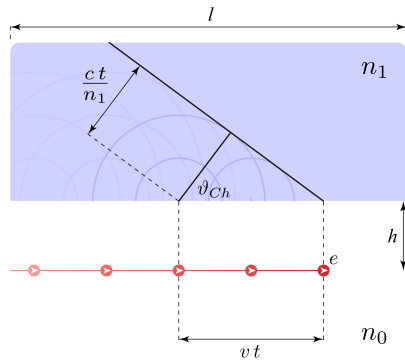


Figure 17: A particle with charge  $e$  travelling in vacuum along the boundary to a dielectric with refractive index  $n_1$ . The length of the radiator is given as  $l$  and the distance between the particle and the radiator surface is denoted  $h$ . ChDR is emitted at the *Cherenkov angle*  $\vartheta_{Ch}$ .

of the spectrum. To validate the predictions there only exists very little experimental data on ChDR in the incoherent regime [33] and experiments with the coherent part of the spectrum [34] to compare the two different analytical models have not been conclusive. We herein discuss the simulation results of experiments aiming to verify the validity of the two different analytical models by calculating the energy loss of a charged particle due to ChDR.

Both models consider the dielectric as shown in Fig. 17 to be infinitely wide (perpendicular to the plane) with the particle travelling in parallel to the surface of the dielectric. The length  $l$  of the dielectric is restricted for one model, but considered infinite ( $l = \infty$ ) for the other. The infinitely long model [31] we denote *stationary model* hereafter. The model restricted in length [32] we denote as *non-stationary model*. In all presented calculations holds  $n_0 = 1$  and all results are scaled to the same radiator length of  $l = 10$  mm. The variables with the greatest effect concerning photon yield are the particle energy and the impact parameter. The first approach for a possible experimental setup considers relatively high energies with a well-controlled transverse beam size. The second approach considers ultra-high energy electron beams.

At the ATF2 beamline at KEK [35] the horizontal beam size is only around 10  $\mu$ m ( $1\sigma$ ), while still providing a high particle energy above 1 GeV and a high bunch charge of more than 1 nC. In Fig. 18 the expected photon yield for the visible spectrum (400–700 nm) from the two models is shown for beam parameters resembling the ATF2 beamline. The plot shows that the expected photon yield per cm of dielectric for the non-stationary model (orange trace) is in the order of magnitude one could expect from particles in the halo [35] producing direct *Cherenkov radiation* (red trace). At distances of around 0.5 mm the non-stationary model predicts nearly  $10^5$  photons per bunch being emitted as ChDR. The photon yield per cm from the stationary model would be four orders of magnitude lower than that.

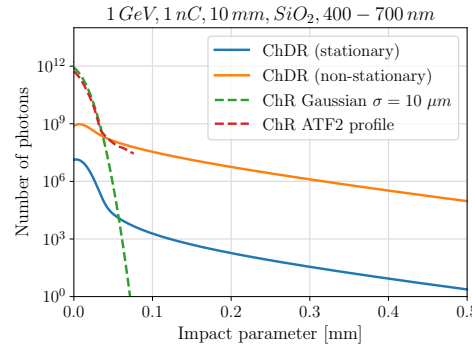


Figure 18: Expected photon yield according to the two different analytical models. The green dotted line corresponds to the photon yield from *Cherenkov radiation* of particles in a *Gaussian* beam hitting the radiator. The red dotted line corresponds to the photon yield from *Cherenkov radiation* considering the beam halo of the ATF2 beam line.

For the second approach, we consider ultra-high energy electrons delivered to the North Area at CERN. As the transverse beam size provided at the North Area is typically in the order of several millimetres the contribution from direct *Cherenkov radiation* on a radiator is too high to discriminate from ChDR. However, as electrons are delivered using a slow extraction scheme from the SPS the possibility remains to track each particle individually. We aim for the highest electron energies without reducing the number of electrons available per spill. The calculated photon yield for 40 and 100 GeV electrons is shown in Fig. 19. With  $10^7$  particles per spill one could expect the production of several hundred photons due to ChDR even at large distances of several millimeters. However, the photon yield predicted by the stationary model would be more than ten orders of magnitude lower than that.

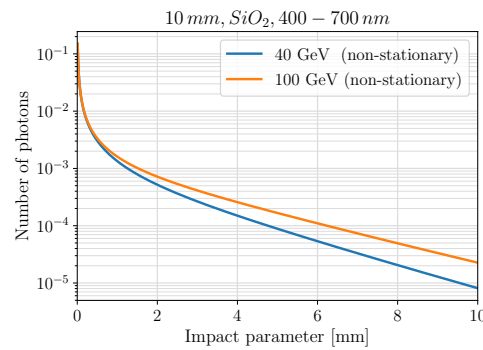


Figure 19: Expected photon yield from ChDR of a single particle calculated using the non-stationary model.

To conclude, the verification of different analytical models presents a challenge given the current test beams even under optimal conditions. We have shown that two different experimental setups might be able to verify the photon yield of ChDR as predicted by the non-stationary model. The

photon yield due to ChDR as predicated by the stationary model is way below that and very unlikely to be measured considering the two different test beams.

### R&D based on Electro-Optical Spectral Decoding

FCC-ee requires a bunch-by-bunch bunch profile monitoring system for its top-up injection and a diagnostics tool based on electro-optical spectral decoding (EOSD) is a possible candidate to fulfill the requirements. At the electron storage ring KARA at KIT, an electro-optical (EO) near-field monitor is installed to perform single shot, turn-by-turn longitudinal bunch profile measurements [36]. It has proven to be a valuable diagnostics tool, which among high-throughput data streaming of single electron bunch profiles [37], is also used for tomography of the longitudinal phase-space [38]. Therefore, the KARA EO diagnostic tools can provide a good foundation for the development of a similar diagnostics system for FCC-ee.

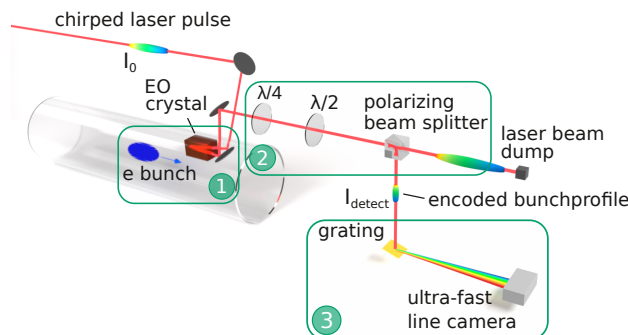


Figure 20: Principle of the EO bunch profile monitor at KARA. Adapted from [38].

Figure 20 shows the principle of the bunch profile monitor at KARA using electro-optical spectral decoding (EOSD), which is best described in three steps: In the first step, the bunch profile is encoded into the polarization of a chirped laser pulse by sending it through an electro-optical crystal next to the electron bunch. The *Coulomb* field of the electrons change the birefringence of the crystal according to the *Pockels* effect, which modulates the polarization of the laser pulse [39]. In the second step, the modulation of the polarization is transformed into an intensity modulation by the use of two waveplates and a polarizing beam splitter in a near-crossed configuration. The third step is a spectrometer containing the KIT-build ultra-fast line camera KALYPSO with a Mfps frame rate [40], which allows turn-by-turn measurements of the spectrum of single laser pulses. Since a chirped laser pulse has been used in the beginning, the intensity modulation in the spectrum corresponds to the temporal charge density profile of a single electron bunch. At KARA, these measurements are performed with an operation mode for short bunches with one single bunch in the ring. However, KARA is also suited for future prototype tests for EOSD at FCC-ee, because the existing EO monitor can be modified and the bunch length and number of bunches can be increased to better fit the beam parameters at FCC-ee.

In order to investigate the challenges for the application of a similar EOSD diagnostic system at FCC-ee, the setup has been replicated in simulations [41]. KARA and FCC-ee machine parameters are different in many ways, but with respect to EOSD, the following particular changes have been identified that need to be addressed: Due to a higher charge density in the bunches, the *Coulomb* fields are up to 10 times stronger than at KARA, depending the operation modes of the accelerators. Strong *Coulomb* fields should be avoided, because it leads to a non-linear relation of the bunch profile and the modulation of the laser pulse. The second major challenge occurs during operation for the production of Z-bosons at an collision energy of 92 MeV, where FCC-ee will have bunch lengths of up to  $\sigma_{\text{FCCee}} z = 15.4 \text{ mm}$  [42]. These bunches are much longer than the typical bunch length during measurements at KARA of around  $\sigma_{\text{KARA}} = 3 \text{ mm}$ .

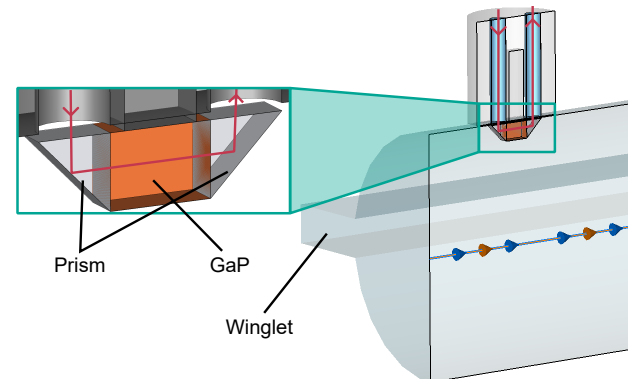


Figure 21: Concept of an adapted EO monitor design for FCC-ee [43].

Therefore, a new conceptual design of the crystal holder has been developed and tested in simulations [43]. In Fig. 21, the adapted design is presented as a 3D model installed in the FCC-ee beam pipe. Compared to the KARA setup, it has a modified laser path through the crystal, which avoids the laser pulse first travelling upstream against the direction of the electron bunch. This modification allows measurements of longer bunches, because it avoids disturbances by an overlapping upstream signal. The KARA design had a metal mirror next to the crystal to guide the laser beam, which has been replaced by prisms for the new design. This is used for the modified laser path and it helps to reduce impedance and disturbances of the *Coulomb* field. By placing the crystal at the edge of the beam pipe, the strength of the *Coulomb* field in the crystal during Z-operation is reduced to a level similar to the KARA setup.

As a result, the simulations show that single bunch EOSD measurements similar to the measurements at KARA can be achieved with the adapted design. Refining, building and testing the prototype design is currently in progress, with the goal to provide a proof-of-principle for an EOSD bunch profile monitor for FCC-ee.

## CONCLUSIONS

An overview of the technical challenges for some of the major beam instrumentation systems for FCC-ee was presented, along with first R&D initiatives and some relevant beam studies. However, beside these technical and scientific challenges, also managerial and funding challenges lie ahead – for both, the FCC-ee BI R&D program and the final realization. It may be worth to mention, past experience show the contribution of the beam instrumentation on the total project costs for hadron colliders was typically in the range 3 . . . 5 %, while for lepton machines like 4<sup>th</sup>-generation synchrotron light sources the BI cost contribution is up to 10 %.

## REFERENCES

- [1] A. Abada *et al.*, “FCC-ee: The Lepton Collider: Future Circular Collider Conceptual Design Report Volume 2,” *Eur. Phys. J. ST*, vol. 228, no. 2, pp. 261–623, 2019. doi: 10.1140/epjst/e2019-900045-4.
- [2] F. Brinker, A. Hagedestad, and M. Wendt, “Precision alignment of bpm’s with quadrupole magnets,” 1996.
- [3] G. Priebe, D. Nölle, M. Wendt, and M. Werner, “Precision alignments of stripline bpm’s with quadrupole magnets for ttf2,” 2004.
- [4] D. Noelle, G. Priebe, M. Wendt, and M. Werner, “BPMs with precise alignment for TTF2,” *AIP Conf. Proc.*, vol. 732, no. 1, T. Shea and R. C. Sibley, Eds., pp. 166–173, 2004. doi: 10.1063/1.1831144.
- [5] S. Zorzetti, M. Wendt, and L. Fanucci, “Study of the Electrical Center of a Resonant Cavity Beam Position Monitor (RF-BPM) and Its Integration with the Main Beam Quadrupole for Alignment Purposes,” in *2nd North American Particle Accelerator Conference*, 2017, FRA2CO03. doi: 10.18429/JACoW-NAPAC2016-FRA2CO03.
- [6] E. Carideo, M. Migliorati, D. De Arcangelis, and I. M. Zobov, “Transverse and longitudinal single bunch instabilities in fcc-ee,”
- [7] M. Migliorati, C. Antuono, E. Carideo, Y. Zhang, and M. Zobov, “Impedance modelling and collective effects in the future circular e $\Theta$ -e $\Theta$  collider with 4 ips,” *arXiv preprint arXiv:2204.04616*, 2022.
- [8] M. Kastriotou *et al.*, “BLM Crosstalk Studies on the CLIC Two-Beam Module,” in *Proc. of International Beam Instrumentation Conference (IBIC2015), Melbourne, Australia, 13-17 September 2015*, (Melbourne, Australia), M. Boland, D. Button, K. Riches, and V. R. Schaa, Eds., ser. International Beam Instrumentation Conference, JACoW, Geneva, Switzerland: JACoW, Jan. 2016, pp. 148–151, ISBN: 978-3-95450-176-2. doi: 10.18429/JACoW-IBIC2015-MOPB045. <http://accelconf.web.cern.ch/AccelConf/IBIC2015/papers/mopb045.pdf>
- [9] E. Nebot Del Busto *et al.*, “Position Resolution of Optical Fibre-Based Beam Loss Monitors Using Long Electron Pulses,” in *Proc. of International Beam Instrumentation Conference (IBIC2015), Melbourne, Australia, 13-17 September 2015*, (Melbourne, Australia), M. Boland, D. Button, K. Riches, and V. R. Schaa, Eds., ser. International Beam Instrumentation Conference, JACoW, Geneva, Switzerland: JACoW, Jan. 2016, pp. 580–584, ISBN: 978-3-95450-176-2. doi: 10.18429/JACoW-IBIC2015-WEZAS03. <http://accelconf.web.cern.ch/AccelConf/IBIC2015/papers/webla03.pdf>
- [10] M. Kastriotou *et al.*, “A Versatile Beam Loss Monitoring System for CLIC,” in *Proc. of International Particle Accelerator Conference (IPAC’16), Busan, Korea, May 8-13, 2016*, (Busan, Korea), ser. International Particle Accelerator Conference, doi:10.18429/JACoW-IPAC2016-MOPMR024, Geneva, Switzerland: JACoW, Jun. 2016, pp. 286–289, ISBN: 978-3-95450-147-2. doi: doi : 10 . 18429 / JACoW - IPAC2016 - MOPMR024. <http://jacow.org/ipac2016/papers/mopmr024.pdf>
- [11] G. Mitsuka, H. Ikeda, and T. Mitsuhashi, “Renovation of the SR Beam Profile Monitors with Novel Polycrystalline Diamond Mirrors at the SuperKEKB Accelerator,” in *Proc. IPAC’22*, (Bangkok, Thailand), ser. International Particle Accelerator Conference, JACoW Publishing, Geneva, Switzerland, Jul. 2022, MOPOPT031, pp. 313–315, ISBN: 978-3-95450-227-1. doi: 10 . 18429 / JACoW - IPAC2022 - MOPOPT031. <https://jacow.org/ipac2022/papers/mopopt031.pdf>
- [12] G. Mitsuka, H. Ikeda, and T. Mitsuhashi, “Design and Construction of Optical System of the Coronagraph for Beam Halo Observation in the SuperKEKB,” in *Proc. IPAC’22*, (Bangkok, Thailand), ser. International Particle Accelerator Conference, JACoW Publishing, Geneva, Switzerland, Jul. 2022, TUOXGD1, pp. 769–771, ISBN: 978-3-95450-227-1. doi: 10 . 18429 / JACoW - IPAC2022 - TUOXGD1. <https://jacow.org/ipac2022/papers/tuoxgd1.pdf>
- [13] T. Mitsuhashi, K. Oide, and F. Zimmermann, “Conceptual Design for SR Monitor in the FCC Beam Emittance (Size) Diagnostic,” in *Proc. of International Particle Accelerator Conference (IPAC’16), Busan, Korea, May 8-13, 2016*, (Busan, Korea), ser. International Particle Accelerator Conference, doi:10.18429/JACoW-IPAC2016-MOPMB022, Geneva, Switzerland: JACoW, Jun. 2016, pp. 133–136, ISBN: 978-3-95450-147-2. doi: doi : 10 . 18429 / JACoW - IPAC2016 - MOPMB022. <http://jacow.org/ipac2016/papers/mopmb022.pdf>
- [14] M. Boland, T. Mitsuhashi, and K. Wootton, “Turn-by-turn observation of the injected beam profile at the australian synchrotron storage ring,” vol. IBIC2012, Geneva, Switzerland: JACoW, 2012, pp. 276–278, ISBN: 978-3-95450-119-9.
- [15] H. Ikeda, T. Mitsuhashi, and G. Mitsuka, “Injection Beam Measurement Using Synchrotron Radiation Monitor at the SuperKEKB Electron Ring,” in *Proc. IPAC’22*, (Bangkok, Thailand), ser. International Particle Accelerator Conference, JACoW Publishing, Geneva, Switzerland, Jul. 2022, FROXGD3, pp. 3121–3123, ISBN: 978-3-95450-227-1. doi: 10 . 18429 / JACoW - IPAC2022 - FROXGD3. <https://jacow.org/ipac2022/papers/froxgd3.pdf>
- [16] M. Siano *et al.*, “Two-dimensional electron beam size measurements with x-ray heterodyne near field speckles,” *Phys. Rev. Accel. Beams*, vol. 25, p. 052801, 2022.
- [17] M. Siano, B. Paroli, and M. A. C. Potenza, “Heterodyne near field speckles: From laser light to x-rays,” *Advances in Physics: X*, vol. 6, p. 1891001, 2021.
- [18] M. D. Alaimo *et al.*, “Probing the transverse coherence of an undulator x-ray beam using brownian particles,” *Phys. Rev. Lett.*, vol. 103, p. 194805, 2009.
- [19] M. Siano *et al.*, “Characterizing temporal coherence of visible synchrotron radiation with heterodyne near field speckles,” *Phys. Rev. Accel. Beams*, vol. 20, p. 110702, 2017.

- [20] J. W. Goodman, *Statistical Optics*. John Wiley & Sons, Inc., New York, 2000.
- [21] M. Siano *et al.*, “Focus: Fast monte carlo approach to coherence of undulator sources,” *Proceedings of the 11th International Beam Instrumentation Conference IBIC 2022*, 2022.
- [22] L. J. Nevay *et al.*, “Laserwire at the accelerator test facility 2 with submicrometer resolution,” *Phys. Rev. ST Accel. Beams*, vol. 17, p. 072 802, 7 Jul. 2014. doi: 10.1103/PhysRevSTAB.17.072802. <https://link.aps.org/doi/10.1103/PhysRevSTAB.17.072802>
- [23] A. Blondel *et al.*, “Polarization and Centre-of-mass Energy Calibration at FCC-ee,” Sep. 2019. arXiv: 1909.12245 [physics.acc-ph].
- [24] A. Jeff *et al.*, “Longitudinal density monitor for the lhc,” *Phys. Rev. ST Accel. Beams*, vol. 15, p. 032 803, 3 Mar. 2012. doi: 10.1103/PhysRevSTAB.15.032803. <https://link.aps.org/doi/10.1103/PhysRevSTAB.15.032803>
- [25] C. P. Welsch *et al.*, “Longitudinal beam profile measurements at ctf3 using a streak camera,” *Journal of Instrumentation*, vol. 1, no. 09, P09002, Sep. 2006. doi: 10.1088/1748-0221/1/09/P09002. <https://dx.doi.org/10.1088/1748-0221/1/09/P09002>
- [26] A. Curcio *et al.*, “Noninvasive bunch length measurements exploiting cherenkov diffraction radiation,” *Phys. Rev. Accel. Beams*, vol. 23, p. 022 802, 2 Feb. 2020. doi: 10.1103/PhysRevAccelBeams.23.022802. <https://link.aps.org/doi/10.1103/PhysRevAccelBeams.23.022802>
- [27] T. Obina and T. Mitsuhashi, “Measurement of bunch lengthening effects using a streak camera with reflective optics,” vol. DIPAC2007, Geneva, Switzerland: JACoW, 2007, pp. 256–258, ISBN: 978-3-95450-011-6.
- [28] M. Boland, T. Mitsuhashi, and Y. Tan, “Reflective Streak Camera Bunch Length Measurements at the Australian Synchrotron,” in *Proc. 5th International Particle Accelerator Conference (IPAC’14), Dresden, Germany, June 15–20, 2014*, (Dresden, Germany), ser. International Particle Accelerator Conference, <https://doi.org/10.18429/JACoW-IPAC2014-THPME080>, Geneva, Switzerland: JACoW, Jul. 2014, pp. 3421–3423, ISBN: 978-3-95450-132-8. doi: <https://doi.org/10.18429/JACoW-IPAC2014-THPME080>. [http://jacow.org/ipac2014/papers/thpme080.pdf](https://jacow.org/ipac2014/papers/thpme080.pdf)
- [29] H. Obina *et al.*, “Vertical beam size measurement by streak camera under colliding and single beam conditions in kekb,” vol. PAC2005, IEEE, 2005, pp. 31 294–3196, ISBN: 0-7803-8860-7.
- [30] I. M. Frank and I. E. Tamm, “Coherent visible radiation of fast electrons passing through matter,” *Compt. Rend. Acad. Sci. URSS*, vol. 14, no. 3, pp. 109–114, 1937. doi: 10.3367/UFNr.0093.196710o.0388.
- [31] R. Ulrich, “Zur Cerenkov-Strahlung von Elektronen dicht über einem Dielektrikum,” *Zeitschrift fur Physik*, vol. 194, no. 2, Apr. 1966. doi: 10.1007/BF01326045.
- [32] A. Potylitsyn and S. Gogolev, “Radiation losses of the relativistic charge moving near a dielectric radiator,” *Russian Physics Journal*, vol. 62, Apr. 2020. doi: 10.1007/s11182-020-01965-0.
- [33] R. Kieffer *et al.*, “Direct observation of incoherent cherenkov diffraction radiation in the visible range,” *Phys. Rev. Lett.*, vol. 121, p. 054 802, 5 Aug. 2018. doi: 10.1103/PhysRevLett.121.054802. <https://link.aps.org/doi/10.1103/PhysRevLett.121.054802>
- [34] K. Lasocha *et al.*, “Experimental Verification of Several Theoretical Models for ChDR Description,” in *Proc. IPAC’22*, (Bangkok, Thailand), ser. International Particle Accelerator Conference, JACoW Publishing, Geneva, Switzerland, Jul. 2022, THOYGD1, pp. 2420–2423, ISBN: 978-3-95450-227-1. doi: 10.18429/JACoW-IPAC2022-THOYGD1. <https://jacow.org/ipac2022/papers/thoygd1.pdf>
- [35] R. Yang *et al.*, “Evaluation of beam halo from beam-gas scattering at the kek accelerator test facility,” *Phys. Rev. Accel. Beams*, vol. 21, p. 051 001, 5 May 2018. doi: 10.1103/PhysRevAccelBeams.21.051001. <https://link.aps.org/doi/10.1103/PhysRevAccelBeams.21.051001>
- [36] N. Hiller *et al.*, “A Setup for Single Shot Electro Optical Bunch Length Measurements at the ANKA Storage Ring,” in *Proc. IPAC’11*, (San Sebastian, Spain, Sep. 2011), JACoW Publishing, Geneva, Switzerland, pp. 1206–1208. <https://jacow.org/IPAC2011/papers/TUPC086.pdf>
- [37] S. Funkner *et al.*, “High throughput data streaming of individual longitudinal electron bunch profiles,” *Physical Review Accelerators and Beams*, vol. 22, no. 2, p. 022 801, Feb. 2019. doi: 10.1103/physrevaccelbeams.22.022801.
- [38] S. Funkner *et al.*, “Revealing the dynamics of ultrarelativistic non-equilibrium many-electron systems with phase space tomography,” *arXiv preprint*, doi: 10.48550/arXiv.1912.01323.
- [39] I. Wilke, A. M. MacLeod, W. A. Gillespie, G. Berden, G. M. H. Knippels, and A. F. G. van der Meer, “Single-Shot Electron-Beam Bunch Length Measurements,” *Physical Review Letters*, vol. 88, no. 12, p. 124 801, Mar. 2002. doi: 10.1103/physrevlett.88.124801.
- [40] M. Patil *et al.*, “Ultra-Fast Line-Camera KALYPSO for fs-Laser-Based Electron Beam Diagnostics,” *Proceedings of the 10th International Beam Instrumentation Conference*, vol. IBIC2021, Re of Korea, 2021. doi: 10.18429/JACoW-IBIC2021-M00B01.
- [41] M. Reißig *et al.*, “Development of an Electro-Optical Longitudinal Bunch Profile Monitor at KARA Towards a Beam Diagnostics Tool for FCC-ee,” in *Proc. IPAC’22*, (Bangkok, Thailand), ser. International Particle Accelerator Conference, JACoW Publishing, Geneva, Switzerland, Jul. 2022, pp. 296–299, ISBN: 978-3-95-450227-1. doi: 10.18429/JACoW-IPAC2022-MOPOPT025.
- [42] K. Oide. “ $\beta_x^*$  = 10cm optics for Z,” 151st FCC-ee Optics Design Meeting. (May 17, 2022), [https://indico.cern.ch/event/1118299/contributions/4766789/attachments/2409541/4122785/Bx%5C%2A10cm\\_Oide\\_220317.pdf](https://indico.cern.ch/event/1118299/contributions/4766789/attachments/2409541/4122785/Bx%5C%2A10cm_Oide_220317.pdf)
- [43] M. Reissig *et al.*, “Status of a Monitor Design for Single-Shot Electro-Optical Bunch Profile Measurements at FCC-ee,” (Kraków, Poland, Sep. 2022), presented at IBIC’22, Kraków, Poland, Sep. 2022, paper WEP26, unpublished.